ELSEVIER

Thin Solid Films 327–329 (1998) 150–155

thin solid films

Structure of SAMs generated from functionalized thiols on gold

K. Tamada[a,*], J. Nagasawa[a], F. Nakanishi[a], K. Abe[a], M. Hara[b], W. Knoll[b], T. Ishida[c], H. Fukushima[d], S. Miyashita[d], T. Usui[d], T. Koini[e], T. R. Lee[e]

[a]*National Institute of Materials and Chemical Research (NIMC), Tsukuba, Ibaraki 305, Japan*
[b]*Frontier Research Program, RIKEN, Wako, Saitama 351-01, Japan*
[c]*Joint Research Center for Atom Technology (JRCAT), Tsukuba, Ibaraki 305, Japan*
[d]*SEIKO-EPSON Co., Suwa, Nagano 392, Japan*
[e]*University of Houston, Houston, TX 77204-5641, USA*

Abstract

The structure and growth of two classes of self-assembled monolayers (SAMs) on Au(111) derived from the adsorption of the functionalized thiol hexyl-azobenzenethiol (12-(4-(4-hexylphenylazo)phenoxy)dodecane-1-thiol) and the partially fluorinated alkanethiols $(CF_3(CF_2)_9(CH_2)_{11}SH$ and $CF_3(CF_2)_7(CH_2)_6SH$ were examined. The structural properties of the SAMs were strongly influenced by the interactions between the functional groups comprising the tails of the molecules. Molecular resolution atomic force microscopy (AFM) images of the hexyl-azobenzenethiol SAMs revealed an expanded lattice (nearest neighbor spacing, $a = 0.53$ nm, $b = 0.56$ nm, and angle between the two axes, $\varphi = 85°$) relative to those of simple azobenzene-terminated SAMs. The expanded lattice probably results from the presence of the hexyl tail groups. The structure of the SAMs formed from the fluorinated alkanethiols was also probed by AFM, Fourier transform infrared spectroscopy (FTIR-RAS) and dynamic contact angle measurements. The degree of molecular tilt of the fluorocarbon helix appears to be influenced by the length of the methylene spacer moieties, which might result from the introduction of flexibility into the molecular chains.

Keywords: Monolayers; Atomic force microscopy; Gold

1. Introduction

Self-assembled monolayers (SAMs) derived from alkanethiols adsorbed on Au(111) have been widely studied during the past 10 years with various surface characterization techniques [1,2]. As an outcome, the fundamental characteristics of these SAMs are becoming more completely understood. Although the molecule ordering in SAMs is largely governed by molecular-substrate interactions, lateral chain–chain interactions are also quite important. In some cases, SAMs with short alkyl chains exhibit quite different film characteristics than those with long alkyl chains [3–5]. However, not only are the van der Waals interactions between alkyl chains small compared with the strength of the Au–S bond [6,7], they are also smaller than the binding energy differences afforded by the spatial modulation of the gold lattice [8]. The fact that the structure of chemisorbed films can be influenced by these small chain-chain interactions can be interpreted by regarding the SAMs as being far from equilibrium during the growth process. It is no doubt that the lateral interactions play a key role in the molecular rearrangement at the 'physisorption' stage [9], and they may be responsible for the formation of metastable structures as well. These kinetically trapped structures can be relaxed or rearranged at the 'chemisorption' stage. However, in practice, because of kinetic barriers and slow diffusion on the solid surface, these metastable structures can be readily observed.

In this article, we report the structure and growth of two new types of SAMs on Au(111), which are derived from newly synthesized compounds in our groups, 'hexyl-azobenzenethiol' (12-(4-(4-hexylphenylazo)phenoxy)dodecane-1-thiol) and partially fluorinated alkanethiols ($(CF_3\ (CF_2)_9(CH_2)_{11}SH$: 'F10H11SH', $CF_3(CF_2)_7(CH_2)_6SH$: 'F8H6SH') (Scheme 1). Due to the nature of the tail groups, these SAMs are expected to have different molecular packings from those derived from simple alkanethiols. For

* Corresponding author. Tel: +81 298 544673; fax: +81 298 544673; e-mail: tamada@nimc.go.jp

0040-6090/98/$ - see front matter
PII S0040-6090(98)00618-X

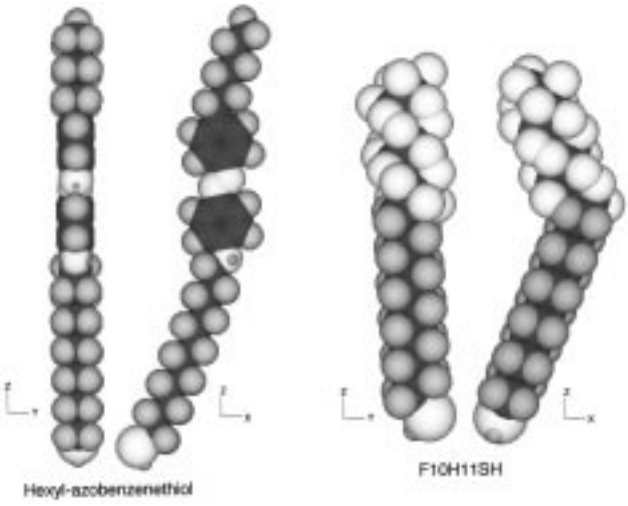

Scheme 1. The molecular conformations of hexyl-azobenzenethiol and fluorinated alkanethiol (F10H11SH) estimated from energy optimizations from force-field calculations (MM2).

example, azobenzene-containing amphiphiles are known to exhibit J or H type aggregation due to the specific intermolecular interactions between dye moieties [10]. The film structure of azobenzene-terminated thiols on Au(111) has been reported [11–13]. These films exhibit incommensurate lattices with the underlying Au(111), having much smaller unit cells (hexagonal lattice with 4.50 ± 0.06 Å nearest neighbor spacing [12,13]) than that of alkanethiol SAMs ($\sqrt{3} \times \sqrt{3}$R30 lattice with 5.00 ± 0.02 Å nearest neighbor spacing [14]). A 'bundle model' that rationalizes the experimental results has been proposed [12,13]. Following these results, the introduction of a terminal hexyl group to the azobenzene unit might lead to significant changes in the film characteristics. This hexyl-azobenzenethiol SAM holds additional interest in the study and development of aligned liquid crystal (LC) films [15]. These studies show that the hexyl-terminal groups in the *para*-position effectively induce the LC alignment changes between homeotropic and planar modes as a result of *trans* and *cis* photoisomerization of the azobenzene unit. In other studies, SAMs derived from fluorinated alkanethiols are expected to exhibit unique molecular packing due to the steric influence of the bulky head groups composed of helical perfluorocarbon chains (van der Waals diameter of 5.6 Å [16]). These fluorinated SAMs are also of particular interest as model surfaces of poly(tetrafluoroethylene) (PTFE), i.e. as extremely low energy and highly hydrophobic (low wetting) surfaces [17]. The influence of the alkyl chain length (spacer group) on the molecular tilt is reported herein.

2. Experimental

Au(111)/mica substrates were prepared by the epitaxial growth of 100–150 nm gold films onto freshly cleaved mica sheets in a vacuum chamber (BIEMTRON). Gold was thermally deposited on the mica surface prebaked at 550°C for 3 h. Deposition was carried out at a rate of 1 A/s and a substrate temperature of 350°C under a vacuum pressure of 10^{-7}–10^{-8} Torr. After deposition, the substrates were annealed at 550°C for ~3 h. This procedure produced an atomically flat Au(111) surface with crystal grains measuring 500–1000 nm in diameter [9]. Au(111) substrates were removed from the vacuum chamber immediately before use, and immersed into freshly prepared thiol solutions within 10 min after exposure to air. The synthesis of 'hexyl-azobenzenethiol' (12-(4-(4-hexylphenylazo)phenoxy)dodecane-1-thiol) and partially fluorinated alkanethiols ($(CF_3(CF_2)_9(CH_2)_{11}SH$: F11011SH, $CF_3(CF_2)_7(CH_2)_6SH$: F_8H_6SH) is described elsewhere [18]. For the kinetics studies, Au(111)/mica substrates (1×1 cm) were immersed into 10^{-2} mM thiol solutions for different immersion times (30 s, 1 min, 3 min, 1 h) at room temperature. These immersion times were chosen following previous kinetics studies of alkanethiol adsorption on Au(111) [9,19,20]. At the designated times, the substrates were quickly removed from the solutions and immediately rinsed with absolute CH_2Cl_2 (10 s~1 h), and dried in a stream of N_2 gas. We prepared the 'equilibrium' surface by exposing the gold substrate to a 1 mM solution for over 24 h at room temperature. This condition is believed to generate fully adsorbed SAMs on Au(111) from alkanethiols [19].

The atomic force microscopy (AFM) system used in this study was a commercially available NanoScope III (Digital Instruments, Santa Barbara, CA). The measurements were performed in contact mode (30 μm scanner) in air at room temperature. The Si_3N_4 cantilever with a spring constant of 0.12 N/m was used for large-sized scans (scanning rate = 3–10 Hz), while a cantilever with a spring constant of 0.38 N/m was used for molecular resolution imaging (scanning rate = 10–30 Hz). All images (400×400 pixels) were collected in the 'height mode', which kept the force constant. The applied force was minimized during the AFM imaging by adjusting the 'set point voltage' to the lower limit [9]; the images were not significantly affected unless the applied force was more than 50 nN.

X-ray photoelectron spectroscopy (XPS) measurements were carried out using an ESCALAB 220iXL system (VG Scientific) with a monochlomatic Al K_α X-ray source (1487 eV). The binding energies were corrected using a Au(4f7/2) peak energy (84.0 eV) as an energy standard. The pass energy of the analyzer was set at 20 eV. Fitting of the XPS peaks was performed using the spectra processing program in the XPS software.

Infrared spectra of the SAMs were taken in the reflection mode (the incident angle = 80° to the surface normal) using a p-polarized beam and the Perkin–Elmer System 2000FTIR. The spectrometer was purged with dry nitrogen, and a liquid-nitrogen-cooled mercury–cadmiumtelluride (MCT) detector was utilized for the reflection measurements. The spectra were recorded at 4 cm^{-1} resolution with 100–1000 scans in the 4000–800 cm^{-1} region. Bare

Au(111), which was deposited at the same time as the gold used for the SAM substrates, was used as a reference to minimize the experimental error arising from roughness and contamination of the gold surface.

Dynamic contact angle measurements were performed using the Wilhelmy plate method with a Cahn balance (DCA322 model). We used a modified technique to measure the asymmetric Au–thiol SAM plates (surface: Au–thiol SAMs, back: cleaved mica, substrate size: 1 cm × 2 cm × 50 μm) [21,22]. The Wilhelmy plate method is recognized as the most favorable technique to measure dynamic contact angles because it allows the measurement of wide surfaces (~cm across) without operator error, and both the advancing and receding speeds can be controlled with a DC motor drive. All measurements utilized pure water at room temperature, and an advancing and receding speed of 20 μm/s.

3. Results and Discussion

3.1. Adsorption kinetics of hexyl-azobenzenethiol

The kinetics of adsorption of hexyl-azobenzenethiol was followed by XPS [23]. Fig. 1 plots the surface coverage calculated from the peak area of C(1s) signal, versus the immersion time, where the data have been normalized by setting the peak area of fully adsorbed SAMs (1 mM, 24 h immersion) to unity. The kinetics of the adsorption of hexyl-azobenzenethiols on Au(111) was quite similar to the kinetics of SAM formation from simple alkanethiols, where sub-monolayers (partially covered surfaces) were obtained in less than 10 min of immersion at concentrations of 10^{-2} mM [9]. Fig. 2 shows the surface morphologies of the sub-monolayers formed by immersion for 30 s, 1 min and 3 min in the 10^{-2} mM solution. Similar to SAMs from octadecanethiol, island formation could be observed, and the area fraction of the domain phases increased as the immersion time increased [9].

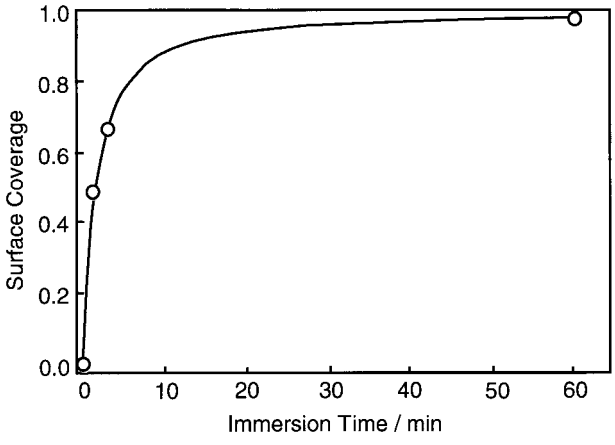

Fig. 1. Adsorption kinetics of hexyl-azobenzenethiol on Au(111) at a solution concentration of 10^{-2} mM, estimated from the C(1s) signal intensities.

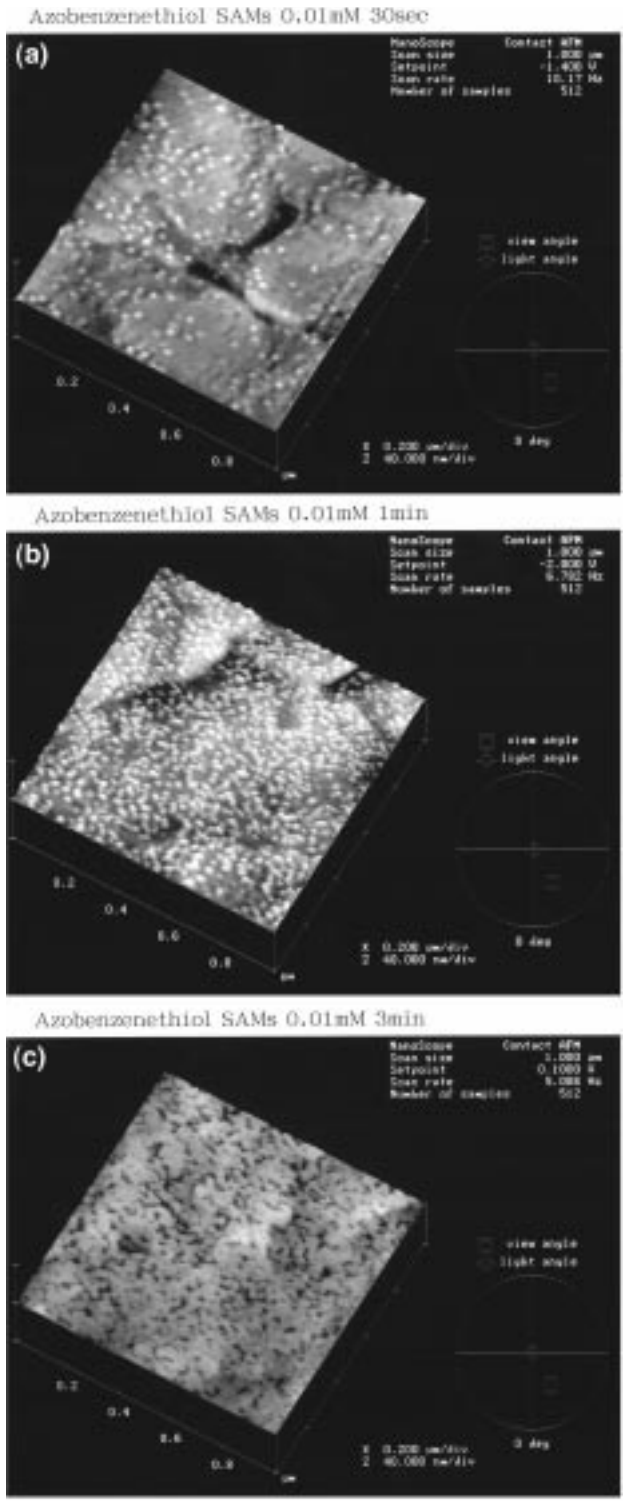

Fig. 2. AFM images of hexyl-azobenzenethiol SAMs on Au(111) at different immersion times in 10^{-2} mM CH_2Cl_2 solutions: (a) 30s, (b) 1 min, (c) 3 min. In the images, the brighter regions correspond to the condensed thiol islands (liquid or solid phase), and the darker regions correspond to the dilute phase (gas phase or bare Au(111) surface).

3.2. Molecular ordering of hexyl-azobenzenethiol SAMs

To confirm the film density and homogeneity of fully adsorbed SAMs (1 mM, 24 h immersion), we analyzed

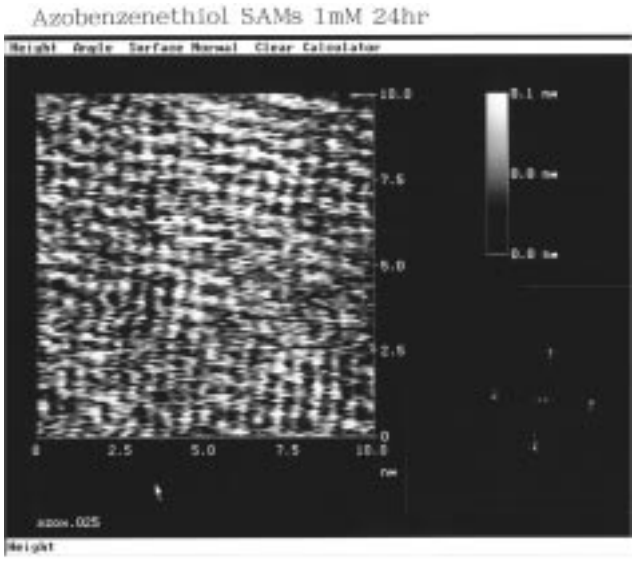

Fig. 3. AFM image and the corresponding 2D Fourier transform of hexyl-azobenzenethiol SAMs on Au(111) covering 10×10 nm^2 (unfiltered), showing a surface lattice with nearest neighbor spacings, $a = 0.53$ nm, $b = 0.56$ nm and angle $\varphi = 85°$.

the system using dynamic contact angle measurements. From the hysteresis loop of the dynamic contact angles for hexyl-azobenzenethiol SAMs on Au(111), an advancing angle (θ_a) of $107.5 \pm 1.0°$ and a receding angle (θ_r) of $97.0 \pm 1.0°$ were obtained. The low wettability and the small hysteresis ($\theta = \theta_a - \theta_r \cong 10°$) are typical for well-ordered alkanethiol SAMs on Au (e.g. C18S/Au: $\theta_a = 112 \pm 1.5°$, $\theta_r = 100.5 \pm 1.5°$; C12S/Au:$\theta_a = 108°$, $\theta_r = 99°$ [24,25]). The contact angles of the azobenzene-terminated SAMs exhibited much lower values ($\theta_a = 89 \pm 1°$, $\theta \cong 10°$ [11]), which can be rationalized by the fact that these monolayers expose aromatic groups rather than alkyl groups to the interface.

Fig. 3 shows the high resolution AFM image of the hexyl-azobenzenethiol SAMs (1 mM, 24 h immersion). The molecular domains exhibiting regular lattice structure were extended over several tens of nanometers on the surface. An oblique lattice with nearest neighbor spacings, $a = 5.3 \pm 0.1$ Å, $b = 5.6 \pm 0.1$ Å, and angle between the two axes $\varphi = 85 \pm 1°$ was confirmed by the Fourier transform of the SAM images. The unit cell can be described as $a = 7.4$ Å, $b = 8.0$ Å, $\varphi = 87°$ by crystallographic description (the basic unit cell contains two molecules). A different type of lattice (distorted hexagonal, $a = 5.5$ Å) could also be observed in some cases. The nearest neighbor distance, however, was similar for both types of lattices. These lattice constants are distinctly larger than those of azobenzene-terminated SAMs (4.50 ± 0.06 Å (hexagonal) and 4.36 ± 0.05 Å, 85° (oblique) [12,13]). As described before, the azobenzene-terminated SAMs formed incommensurate lattices due to strong aromatic interactions between azobenzene units ('bundle model', see Fig. 4 [12,13]). For our hexyl-azobenzenethiol SAMs, the drive to maximize van der Waals contact between terminal hexyl groups attached to the para-position of the azobenzene units probably causes the expansion of lattice. Langmuir–Blodgett (LB) films composed of azobenzene derivatives with terminal alkyl groups (6-(4-(4-octylpheny-lazo)phenoxy)hexanoic acid) exhibit a similar lattice structure (distorted monoclinic, $a = 6.08 \pm 0.03$ Å, $b = 5.67 \pm 0.03$ Å, $\varphi = 55 \pm 1°$ [26]. These results support the above hypothesis that the terminal hexyl groups participate in the molecular ordering process. Molecular packing models of the hexylazobenzenethiol SAMs are depicted in Fig. 4c, and a more definitive model is described elsewhere with data from Fourier transform infrared spectroscopy (FTIR-RAS) (C–H stretching frequency analysis) and reflection UV-Vis absorption spectroscopy [27].

3.3. Molecular ordering of fluorinated alkanethiol SAMs

The dynamic contact angles of fluorinated alkanethiol SAMs on Au(111), prepared by immersion for 24 h at a concentration of 1 mM, were investigated (F10H11SH: $\theta_a = 122 \pm 2°$, $\theta_r = 117 \pm 1°$; F8H6SH: $\theta_a = 121 \pm 2°$, $\theta_r = 113 \pm 1°$). The low wettabilities of the SAMs derived from both F1OH11SH and F8H6SH are quite reasonable for highly fluorinated surfaces in which CF_3 groups are exposed at the interface [28]. The small hysteresis suggest that these fluorinated alkanethiols formed stable chemisorbed films on Au(111). Analysis by high resolution AFM reveals a distorted hexagonal or oblique lattice with a nearest neighbor distance $\theta = 5.9 \pm 0.1$ Å for both fluorinated SAMs (Fig. 5).

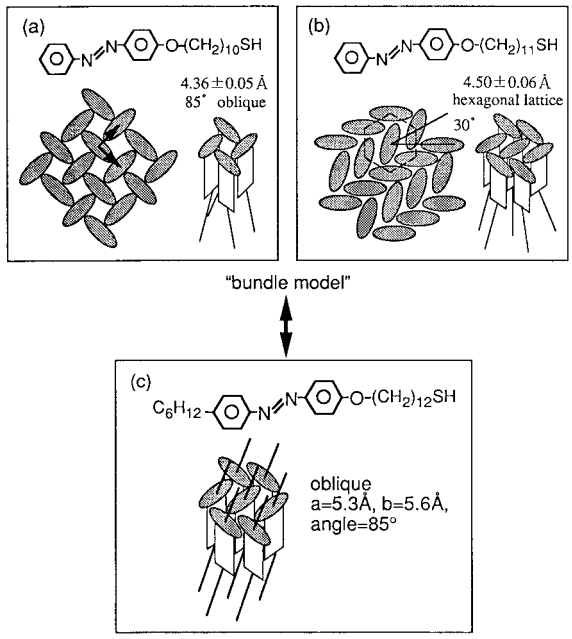

Fig. 4. Molecular packing models of the azobenzene-terminated SAMs on Au (111) proposed by (a) R. Wang, et al. [13]. and (b) W.B. Caldwell, et al. [12]. In both models, the azobenzene terminal groups are spaced ~4.5 Å apart, while the S atoms are assumed to bond in the three-fold hollow sites of Au(111). (c) Illustrates a model for hexyl-azobenzenethiol SAMs in which the molecular lattice is expanded to ~5.5 Å due to the interaction between the hexyl terminal groups.

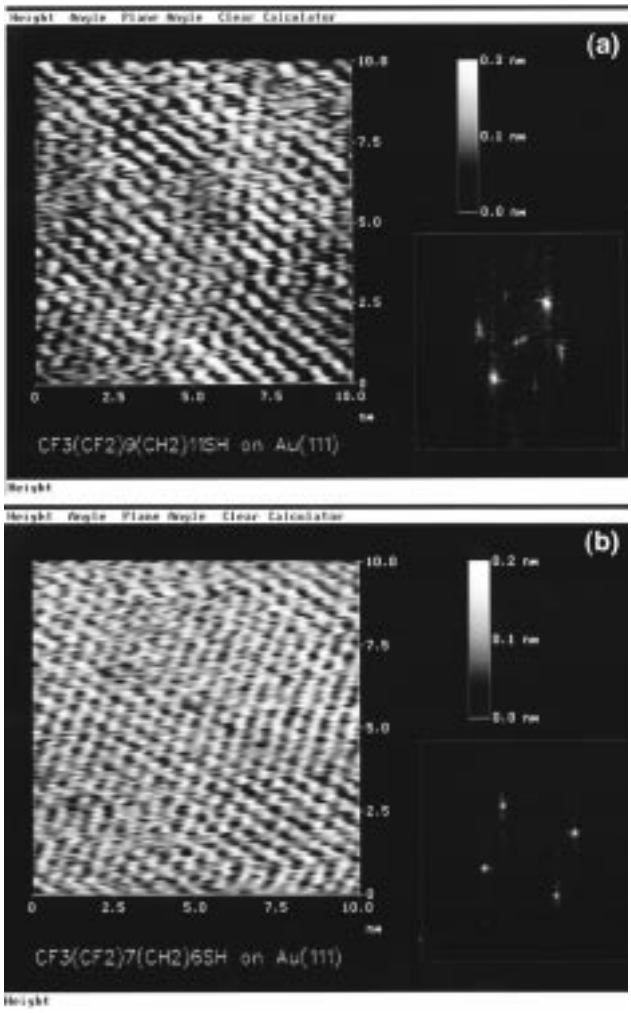

Fig. 5. AFM Image and the corresponding 2D Fourier transform of fluorinated alkanethiol SAMs, (a) F10H11SH and (b) F8H6SH, on Au(111) covering 10×10 nm^2 (unfiltered).

The lattice constant of these SAMs is slightly larger than those derived from fluorinated alkanethiols with fewer methylene spacer groups ($CF_3(CF_2)_n(CH_2)_2SH$) [29,30]. In any case, the bulky perfluorocarbon chain is likely to be responsible for the expansion of these lattices relative to those generated by simple alkanethiols. We observed a difference in the size of the domains of the two new films: the F_8H_6SH SAMs exhibited slightly larger domains with more regular molecular ordering. For both films. the size of domains was in the range of 10–50 nm^2.

We qualitatively explored the molecular orientation of the films with FTIR-RAS by examining the band intensities of the perfluorocarbon chains in the range of 1100–1400 cm^{-1}. Although the origin of a few resonances remain ambiguous [31], most of the bands originating from the perfluorocarbon chains can be assigned based on previous IR studies of PTFE [32,33]. In the present study, we compared the band intensities of asymmetric CF_2 stretching with those of 'axial CF_2' stretching to determine the orientation of the perfluorocarbon chains [31]. The bands at 1210, 1230 and 1150 cm^{-1} result from asymmetric CF_2 stretching [31]. While other bands such as C–C stretching and CCC bending (~1226 cm^{-1}) partially overlap with these bands, the asymmetric CF_2 stretching bands exhibit a change in dipole moment that is perpendicular to the fluorocarbon chain axis. The bands at ~1340 and ~1375 cm^{-1} have been identified as 'axial CF_2' stretching vibrations, which originate from the activation of bands from the interior of the Brillouin zone of the infinite fluorocarbon helix due to the finite length of the CF_2 sequence [31,34]. Perfluorocarbon oligomers, but not PTFE polymers, exhibit these bands in which the change in dipole moment falls along the helical axis. Following these arguments, when the perfluorocarbon chains are oriented parallel to the surface, the relative intensities of the asymmetric CF_2 stretching bands (1210, 1230 and 1150 cm^{-1}) are enhanced relative to the 'axial CF_2' stretching bands (1340 and 1375 cm^{-1}). On the other hand, when the perfluorocarbon chains are oriented perpendicular to the surface, the intensities of the asymmetric CF_2 stretching bands are diminished relative to the 'axial CF_2' stretching bands.

Fig. 6 shows the FTIR-RAS spectra of F1OH11SH and F8H6SH SAMs on Au(111) prepared by immersion for 24 h at a concentration of 1 mM. The F1OH11SH SAMs exhibit more intense asymmetric CF_2 stretching bands than the F8H6SH SAMs. In addition, a previous FTIR-RAS study of a SAM derived from a fluorinated alkanethiol with an even shorter methylene spacer, $CF_3(CF_2)_7(CH_2)_2SH$ (F8H2SH), reveals a spectrum in which the asymmetric CF_2 stretching bands are noticeably weaker than the 'axial CF_2' stretching bands [16]. In the absence of any effects due to the different length of the perfluorocarbon segments (e.g. F10 vs. F8), these data suggest that the perfluorocarbon SAMs generated from F10H11SH are oriented more paral-

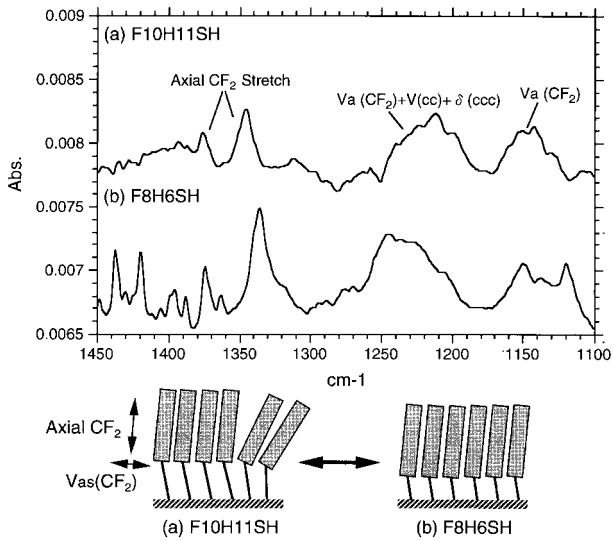

Fig. 6. FTIR-RAS spectra of fluorinated alkanethiol SAMs, (a) F10H11SH and (b) F8H6SH, on Au(111), and the proposed molecular tilt of the fluorocarbon helix predicted by the relative intensities of the axial CF_2 stretching bands (1340 and 1375 cm^{-1}) and the asymmetric CF_2 stretching bands (1210, 1230 and 1150 cm^{-1}).

lel to the surface (i.e. more tilted) than those generated from F8H6SH; both of the SAMs in the present study appear to be more tilted than those generated from F8H2SH [16]. Thus, for partially fluorinated alkanethiol SAMs, it seems that the degree of molecular tilt is influenced by the length of the methylene spacer moieties. This effect might originate from the degree of disorder in the films: in the AFM images described above, the F10H11SH SAMs appear to be more disordered than the F8H6SH SAMs. It is possible that the disorder arises from the introduction of flexibility into the molecular chains as the number of methylene groups is increased. A similar hypothesis was offered in a study of LB films composed of fluorinated fatty acids, where an increase in temperature caused the disordering of perfluorocarbon chains through the 'melting' of long alkyl chains [35].

4. Summary

The structure and growth of two different types of SAMs on gold, hexylazobenzenethiol SAMs and fluorinated alkanethiol SAMs, were examined as a function of the nature of the tail groups. The tail groups were found to have a profound influence on the structure of the SAMs. This knowledge will undoubtedly prove useful in controlling the surface densities and/or lattice structures of SAMs in technological applications that employ these species.

References

[1] A. Ulman (ed.), An Introduction to Ultrathin Organic Films, Academic Press, Boston, MA, 1991.
[2] A. Ulman, Chem Rev. 96 (1996) 1533.
[3] P. Fenter, P. Eisenberger, K.S. Liang, Phys. Rev. Lett. 70 (1993) 2447.
[4] L.H. Dubois, B.R. Zegarski, R.G. Nuzzo, J. Chem. Phys. 98 (1993) 678.
[5] N. Camillone III, T.Y.B. Leung, G. Scoles, Surf. Sci. 373 (1997) 333.
[6] R.G. Nuzzo, B.R. Zegarski, L.H. Dubois, J. Am. Chem. Soc. 109 (1987) 733.
[7] N. Nishida, M. Hara, H. Sasabe, W. Knoll, Jpn. J. Appl. Phys. 35 (1996) 5866.
[8] O.M. Magnussen, B.M. Ocko, M. Deutsh, M.J. Regan, P.S. Pershan, D. Abernathy, G. Grübel, J.-F. Legrand, Nature 384 (1996) 250.
[9] K. Tamada, M. Hara, H. Sasabe, W. Knoll, Langmuir 13 (1997) 1558.
[10] K. Fukuda, H. Nakahara, J. Colloid Interface Sci. 98 (1984) 555.
[11] H. Wolf, H. Ringsdorf, E. Delamarche, T. Takami, H. Kang, B. Michel, Ch. Gerber, M. Jaschke, H.-J. Butt, E. Bamberg, J. Phys. Chem. 99 (1995) 7102.
[12] W.B. Caldwell, D.J. Campbell, K. Chen, B.R. Herr, C.A. Mirkin, A. Malik, M.K. Durbin, P. Dutta, K.G. Huang, J. Am. Chem. Soc. 117 (1995) 6071.
[13] R. Wang, T. Iyoda, L. Jiang, K. Hashimoto, A. Fujishima, Chem. Lett. (1996) 1005.
[14] C.A. Widrig, C.A. Alves, M.D. Porter, J. Am. Chem. Soc. 113 (1991) 2805.
[15] T. Seki, M. Sakuragi, Y. Kawanishi, Y. Suzuki, T. Tamaki, R. Fukuda, K. Ichimura, Langmuir 9 (1993) 211.
[16] C.E.D. Chidsey, D.N. Loacono, Langmuir 6 (1990) 682.
[17] J.R. Dann, J. Colloid Interface Sci. 32 (1970) 302.
[18] T. Koini, M. Graupe, V. Wang, G.M. Nassif, Y. Miura, T.R. Lee in preparation.
[19] C.D. Bain, E.B. Troughton, Y.-T. Tao, J. Evall, G.M. Whitesides, R.G. Nuzzo, J. Am. Chem. Soc. 111 (1989) 321.
[20] M. Buck, F. Eisert, J. Fischer, M. Grunze, F. Träger, Appl. Phys. A 53 (1991) 552.
[21] K. Abe, K. Tamada submitted.
[22] C.D. Volpe, J. Adhes. Sci. Technol. 10 (1994) 1453.
[23] T. Ishida, N. Nishida, S. Tsuneda, M. Hara, H. Sasabe, W. Knoll, Jpn. J. Appl. Phys. 35 (1996) L1710.
[24] H.A. Biebuyck, C.D. Bain, G.M. Whitesides, Langmuir 10 (1994) 1825.
[25] E. Delamarche, B. Michel, H. Kang, Ch. Gerber, Langmuir 10 (1994) 4103.
[26] R. Wang, L. Jiang, T. Iyoda, D.A. Tryk, K. Hashimoto, A. Fujishima, Langmuir 12 (1996) 2052.
[27] K. Tamada, J. Nagasawa, F. Nakanishi, K. Abe, T. Ishida, M. Hara, W. Knoll, Langmuir 14 (1998) 3264.
[28] E.G. Shafrin, W.A. Zisman, J. Phys. Chem. 61 (1957) 1046;64 (1960) 519; 66 (1962) 740.
[29] C.A. Alves, M.D. Porter, Langmuir 9 (1993) 3507.
[30] G.-Y. Liu, P. Fenter, C.E.D. Chidsey, D.F. Ogletree, P. Eisenberger, M. Salmeron, J. Chem. Phys. 101 (1994) 4301.
[31] T.J. Lenk, V.M. Hallmark, C.L. Hoffmann, J.F. Rabolt, D.G. Castner, C. Erdelen, H. Ringsdorf, Langmuir 10 (1994) 4610.
[32] G. Masetti, F. Cabassi, G. Moreli, G. Zerbi, Macromolecules 6 (1973) 700.
[33] H. Vanni, J.F. Tabolt, J. Polym. Sci. Polym. Phys. Ed. 18 (1980) 587.
[34] J.F. Rabolt, T.P. Russell, R.J. Twieg, Macromolecules 17 (1984) 2786.
[35] C. Naselli, J.D. Swalen, J.F. Rabolt, J. Chem. Phys. 90 (1989) 3855.